The Journal of Chemical Physics

RESEARCH ARTICLE | OCTOBER 10 2025

Comprehensive optical spectroscopy of solid-state polymer electrolytes: Harmonic and anharmonic vibrational activity and charge dynamics from terahertz to ultraviolet

Special Collection: Terahertz Spectroscopy

Yuhao Meng ; Jian-Fen Wang ; Matthias Weiling ; Wentao Zhang ; Felix Pfeiffer ; Lukas Goett-Zink ; Tilman Kottke ; Jijeesh Ravi Nair ; Masoud Baghernejad ; Dmitry Turchinovich ; Hassan A. Hafez

J. Chem. Phys. 163, 144903 (2025)
https://doi.org/10.1063/5.0289402

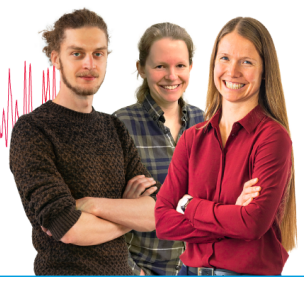

The Journal of Chemical Physics ARTICLE pubs.aip.org/aip/jcp

Comprehensive optical spectroscopy of solid-state polymer electrolytes: Harmonic and anharmonic vibrational activity and charge dynamics from terahertz to ultraviolet

Cite as: J. Chem. Phys. 163, 144903 (2025); doi: 10.1063/5.0289402
Submitted: 7 July 2025 • Accepted: 12 September 2025 •
Published Online: 10 October 2025

Yuhao Meng,[1] Jian-Fen Wang,[2] Matthias Weiling,[2] Wentao Zhang,[1] Felix Pfeiffer,[2] Lukas Goett-Zink,[3,4] Tilman Kottke,[3,4] Jijeesh Ravi Nair,[2,5] Masoud Baghernejad,[2,a)] Dmitry Turchinovich,[1] and Hassan A. Hafez[1,a)]

AFFILIATIONS

[1] Fakultät für Physik, Universität Bielefeld, 33615 Bielefeld, Germany
[2] Helmholtz-Institut Münster, IMD-4, Forschungszentrum Jülich GmbH, 48149 Münster, Germany
[3] Biophysikalische Chemie und Diagnostik, Fakultät für Chemie, Universität Bielefeld, 33615 Bielefeld, Germany
[4] Biophysikalische Chemie und Diagnostik, Medizinische Fakultät OWL, Universität Bielefeld, 33615 Bielefeld, Germany
[5] Department of Digitalization of Resources, Fraunhofer Research Institution for Materials Recycling and Resource Strategies IWKS, Brentanostraße 2a, 63755 Alzenau, Germany

Note: This Paper is Part of the Special Topic: Terahertz Spectroscopy.
[a)]**Authors to whom correspondence should be addressed:** b.masoud@fz-juelich.de and hafez@physik.uni-bielefeld.de

ABSTRACT

We investigate the vibrational and electronic properties of solid-state polymer electrolytes (SPEs) using optical spectroscopy spanning an ultrabroadband range of frequencies extending from terahertz (THz) to ultraviolet (UV). The employed techniques include THz time-domain spectroscopy (THz-TDS), Fourier-transform infrared spectroscopy, and photometric IR–UV spectroscopy. Our study demonstrates that incorporating salts into the host polymer matrix to form an electrolyte gives rise to characteristic optical properties of SPEs, depending on the type, content, and concentration of the added salt, which we describe as follows. In the THz range, distinctive absorption bands are observed, which we attribute to THz-resonant vibrations of polymer chains. In contrast, sharp resonant absorption bands and lines due to IR-active vibrations of chemical bonds (inter- and intra-molecular vibrations) within the polymer chains and lithium salts are observed in the IR range. Density functional theory calculations were performed to provide insight into these vibrational properties of SPEs and helped to assign the relevant vibrational modes. In the UV range, we focus on characterizing the energy gap associated with transitions from bonding to antibonding states. Optical spectroscopy, as a powerful noninvasive characterization tool, thus provides valuable insights into the charge and molecular dynamics in SPEs. These insights are crucial for their technological applications and can support chemistry-based efforts to improve the properties of SPEs.

I. INTRODUCTION

Solvent-free solid polymer electrolytes (SPEs) are regarded as promising candidates for next-generation lithium-ion batteries because they enable the use of lithium metal anodes to reach high energy density and enhance battery safety.[1–3] Among these SPEs, poly(ethylene oxide) (PEO)-based electrolytes have garnered considerable interest due to their ease of fabrication, low toxicity, good electrochemical and thermal stability, and affordability.[2–5] As common energy storage devices, next-generation lithium-ion batteries are anticipated to profoundly impact human life, particularly in areas such as electric vehicles and mobile electronics.[6,7] However,

the ionic conductivity of unmodified SPEs ($<10^{-4}$ S cm^{-1}) is relatively low as compared with that of liquid electrolytes ($>10^{-2}$ S cm^{-1}), limiting their wide commercial application.[3,5] Therefore, improving the ionic conductivity of the SPEs is one of the central tasks in this field.

Typically, SPEs consist of a polymer matrix designed to incorporate lithium salts and can be prepared in either crystalline or amorphous phases.[8] Within this matrix, polar groups such as ethylene oxide (EO) partially coordinate the lithium-ion dissociated from the salts.[9] The transport of lithium-ion occurs along and between the polymer chains, facilitated by their vibrations and segmental motions.[10–13] Recently, a multisalt approach has been proposed to enhance the physical and electrochemical properties of SPEs.[9,14] Using a mixture of two lithium salts, both the ionic conductivity and lithium-ion transference number increase, and better electrochemical stability is achieved.[9] SPEs are complex organic entities that require careful selection of parameters and a delicate balance between various properties to achieve optimal results.[9,15] To guide the optimization of SPEs, a deeper understanding of the molecular and charge dynamics, as well as the synergistic effects between PEO and lithium salts, is essential.

Optical spectroscopy is a versatile characterization tool used across multiple disciplines. By examining the transmission, reflection, or absorption of light, researchers can gain valuable insights into a material's structure, composition, and dynamic processes.[16,17] Here, the electronic and vibrational dynamics of cross-linked PEO-based SPEs are characterized by optical spectroscopy in an ultrawide range of frequencies. In the THz range, THz time-domain spectroscopy (THz-TDS) was carried out to probe the dynamics of polymer chains. These low-frequency dynamics likely correlate with ionic conductivity, as they plausibly facilitate the lithium-ion transport. In the IR range, additional vibrational modes are observed, corresponding to IR-active chemical bond vibrations. To fully interpret the IR spectrum, we consider both fundamental vibrational modes as well as overtones and combination modes enabled by vibration anharmonicity. DFT calculations further support the role of anharmonic responses. IR spectroscopy thus reveals interactions between the functional groups of PEO and lithium salts. Photometric IR–UV spectroscopy aligns well with FTIR spectroscopy at overlapping frequencies and further identifies the energy gap for transitions from bonding to anti-bonding states in the UV range. Hence, the transmissions of four types of samples were measured at room temperature over an ultrabroad range of photon energies, covering three orders of magnitude and extending from 4 meV to 5.9 eV.

II. SAMPLES AND EXPERIMENTS

A. Cross-linked polymer electrolytes

The samples include three cross-linked PEO-based SPEs containing distinctive lithium salts of lithium difluoro(oxalato)borate (LiDFOB), lithium bis(trifluoromethanesulfonyl)imide (LiTFSI), and their mixture, and a pure PEO sample without salts. A solvent-free cross-linked solid polymer electrolyte (XSPE) is synthesized via UV-induced free radical photopolymerization of allyl-terminated poly(ethylene oxide) chains (PEGDAE), along with lithium salts and initiators.[9] The PEGDAE oligomer (n(EO) = 21, MW = 1089 g/mol) is prepared following the method reported by Vijayakumar *et al.*[18] The polymer is melted, mixed with lithium salts, and stirred at 60 °C overnight. After adding a photoinitiator, 2-hydroxy-2-methylpropiophenone (HMPP), and a thermal initiator, the mixture is poured into a Mylar mold, pressed to remove air bubbles, and cooled to form a membrane, with UV curing for 30 min on each side. The samples used in this study are labeled as follows: **X(0):** pure PEO; **X(S1):** PEO containing 25 wt. % LiTFSI; **X(S2):** PEO containing 14 wt. % LiDFOB; and **X(S1+S2):** PEO containing a mixture of 20 wt. % LiTFSI and 3 wt. % LiDFOB. In these electrolytes, the salt dissociates in the PEO matrix, and the Li^+ ions tend to interact with the partially negative oxygen sites of the ether groups in PEO. Then, the ionic conductivity of the electrolyte arises from the hopping of these Li^+ ions along and between the PEO chains, enabled by the PEO chain vibrations.[10–13] All the electrolyte samples, single- and dual-salt-doped samples, exhibit the same EO: Li^+ ratio of 17:1.

B. Ultrabroadband THz-TDS

An in-house built table-top ultrabroadband THz spectrometer based on air-photonics techniques of THz generation and detection was used to characterize the electrolyte samples over the frequency range of 1–25 THz (equivalent to a photon energy range of ~4 to 100 meV and a wavenumber range of ~33.3 to 832.5 cm^{-1}).[19–21] In this experiment, a beam of THz pulses at a repetition rate of 1 kHz was focused by a parabolic mirror at the sample position. The THz fields transmitted through the samples, relative to THz fields obtained via control measurements without samples, were analyzed to obtain their frequency-dependent THz transmission spectra. All measurements were performed in a dry nitrogen environment to avoid the resonant absorption by water molecules of residual humidity. A detailed description of the spectrometer and the associated data analysis is provided in Notes 1 and 2 of the supplementary material.

C. Fourier transform infrared spectroscopy

The FTIR transmission data were measured at room temperature on a Bruker Tensor 27 spectrometer. It is equipped with a room temperature deuterated L-alanine doped triglycine sulfate (DLaTGS) detector, a mid-IR source, and a KBr beamsplitter. Each spectrum, covering the frequency range 500–7500 cm^{-1} (equivalent to a photon energy range of ~0.062 to 0.930 eV), was obtained by accumulating 64 scans per sample, accompanied by 64 background scans, and the resolution of the spectrum was 2 cm^{-1}. The spectra were recorded in a purged environment of dry air to avoid the influence of the vibrational absorption by water molecules of residual humidity.

D. Photometric IR–UV spectroscopy

The photometric IR–UV transmission data were measured at room temperature using a PerkinElmer Lambda 950 spectrometer. Two radiation sources, a deuterium lamp and a halogen lamp, cover the working wavelength range from near-infrared (NIR) to ultraviolet (UV). Source changes occur automatically during monochromator slewing. Holographic gratings are employed in each monochromator for both the ultraviolet/visible (UV/Vis) and NIR ranges. A photomultiplier tube (PMT) detector is used for the UV/Vis range, while a PbS detector is used for the NIR range, with

automatic detector switching during the monochromator slewing. The spectrum covers the range of 210–2640 nm (equivalent to a photon energy range of ~0.470 to 5.904 eV), and the resolution of the spectrum was 5 nm.

III. RESULTS AND DISCUSSION

Figure 1 shows the transmission spectra of the four samples. In the THz range, the transmission is relatively low, indicating a strong absorption. This absorption is even more pronounced in the doped samples, indicating that the lithium salts modify the properties of the SPEs.[10] In the IR range, more vibrational features are observed. The strong, broad absorption bands serve as fingerprints of the fundamental vibrations of chemical bonds.[22] However, fundamental vibrations alone cannot account for all the absorption bands. Through careful comparison and analysis, we propose that the remaining bands likely originate from overtones and combination modes. Further DFT calculations support this suggestion. A sharp transition in the UV region corresponds to the $\pi \rightarrow \pi^*$ electronic transition.[23] In Secs. III A–III D, the spectral features in

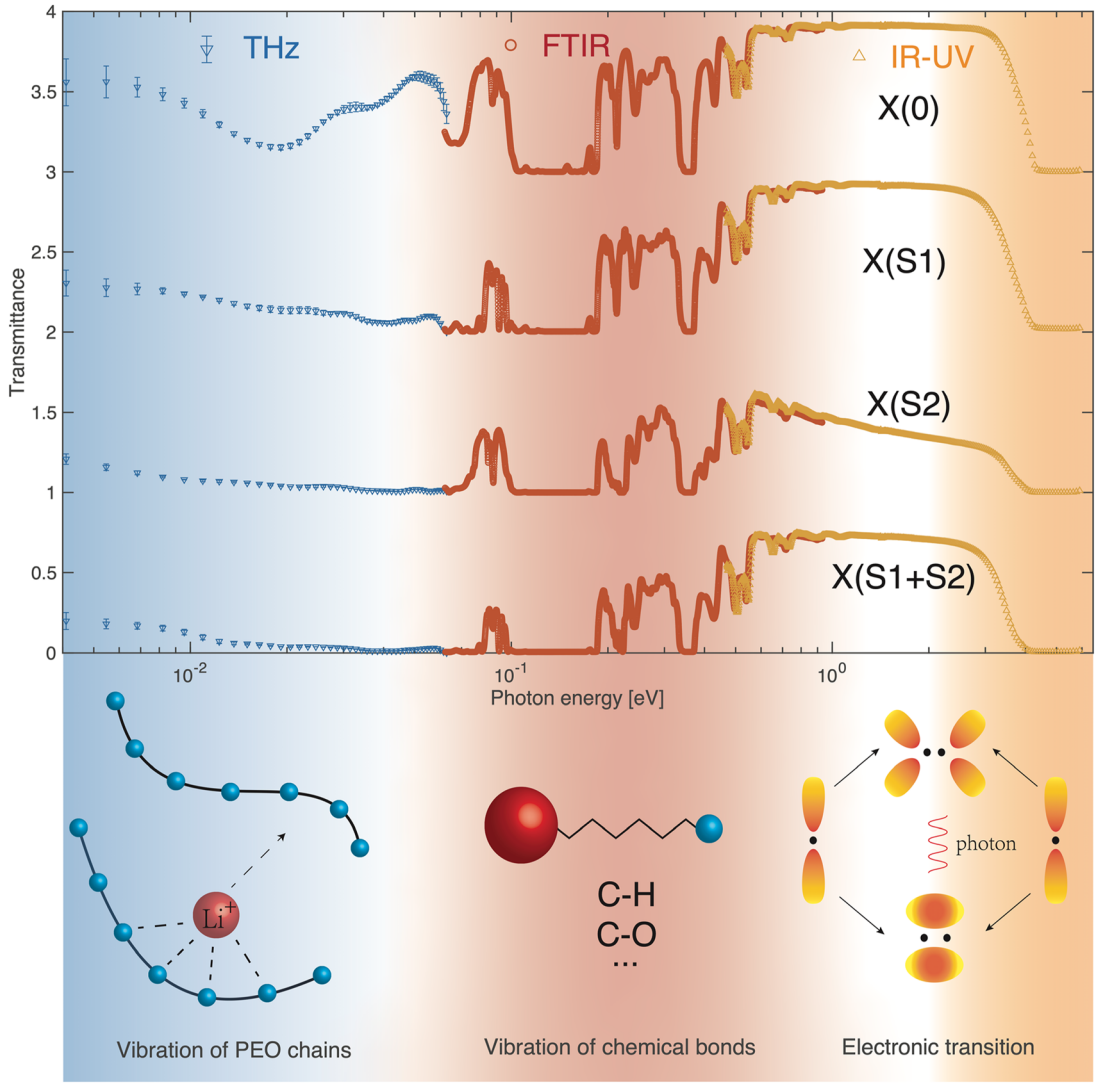

FIG. 1. Transmission spectra of PEO-based SPEs span from the THz to the UV range. At the top, the transmission data for the pure cross-linked polymer X(0), single-salt-doped electrolytes X(S1) [LiTFSI] and X(S2) [LiDFOB], and dual-salt-doped electrolytes X(S1+S2) [LiTFSI+LiDFOB] samples are presented. The vertical axes of different samples have been vertically translated by 1 to aid in distinction. The blue lower triangle data, obtained from ultrabroadband THz spectroscopy, cover a range from 1 THz (0.004 eV) to 15 THz (0.062 eV), with error bars calculated from six measurements. The red circle data are from FTIR experiments, ranging from 500 cm^{-1} (0.062 eV) to 7500 cm^{-1} (0.930 eV). The yellow upper triangle data, from photometric IR–UV measurements, span wavelengths from 2640 nm (0.470 eV) to 210 nm (5.904 eV). At the bottom, schematic diagrams illustrate the main contributions of each spectral range: polymer chain vibrations for the THz range, chemical bond vibrations for the IR range, and electronic transitions from bonding to antibonding states for the UV range.

the three spectral ranges from THz to UV depicted in Fig. 1 are discussed individually.

A. THz spectra

Figure 2 displays the conductivity spectra of the various SPE samples (see the supplementary material, Note 2, for the data analysis). The blue curve represents the conductivity of pure PEO, labeled as X(0). We observe broad absorption bands around 4.6, 9, and 16 THz [Fig. 2(a)], attributed to the vibrations of the PEO chain.[10] With a glass transition temperature of −22 °C, sample X(0) exists in the rubbery semi-crystalline phase at room temperature.[9] THz spectroscopy enables us to capture the local motion of polymer chain segments, which repeatedly create new coordination sites that may serve for ion migration.[8] In the amorphous state, PEO chains have a random arrangement, leading to broader vibrational bands compared to the phonon vibrations in typical crystals.

The addition of lithium salts notably impacts the THz conductivity of PEO, with vibrational absorption bands becoming broader but with larger amplitudes, as compared with those of X(0). This observation aligns with findings that increased salt content renders PEO more amorphous.[9] However, due to the high absorption of SPEs and the phonon absorption inside the silicon wafer filter used in our THz spectrometer, data around 18 THz (highlighted in gray) are unreliable because of low THz intensity (supplementary material, Note 2). Among the single-salt electrolytes, X(S2) exhibits a greater real part of THz conductivity below 15 THz, and its direct current (DC) ionic conductivity also surpasses that of X(S1) (supplementary material, Note 3). The primary mechanism for ionic conductivity at room temperature is the segmental motion of the polymer matrix, which aids in moving ionic species within the electrolyte.[9] The higher THz conductivity and absorption bands broadening suggest increased segmental motion of PEO and reduced crystallinity, respectively, both leading to enhancement of the ionic conductivity of SPEs.[10]

We note here that the bare PEO sample X(0) is entirely an insulator, exhibiting no measurable ionic conductivity. Yet, its THz conductivity (or absorption) is exclusively associated with its chain vibration and relaxation dynamics. On the other hand, the salt doped samples X(S1) and X(S2) exhibit distinct finite electrically measurable ionic conductivities as well as distinguishable THz vibrational dynamics, evidently more pronounced for X(S2), which are attributed to the following. The LiDFOB in X(S2), compared with LiTFSI in X(S1), has a higher solubility in the PEO matrix, enhances the amorphicity of the structure further, and in turn facilitates higher mobility of the Li^+ ions, especially when the temperature increases above the glass temperature.[9,10,24–26] Moreover, molecular dynamic simulations showed that there is a stronger coordination between Li^+ ions and $DFOB^-$ anions than that with $TFSI^-$ anions.[9] In the X(S1) sample, the Li^+ ions are more coordinated with PEO chains, while in the X(S2) and X(S1+S2) samples, the Li^+ ions exhibit balanced coordination with PEO and counteranions. The smaller lithium-ion coordination number with the PEO chain may enhance the vibrational intensity because of less drag effect from the Li^+ ions against the PEO chain motion.[27] This is consistent with our observation that X(S2) and X(S1+S2) have higher THz conductivity than X(S1).

In the dual-salt-doped sample X(S1+S2), even a small amount of LiDFOB (3 wt. %) notably alters the spectra of SPEs. The THz conductivity of X(S1+S2) is comparable to that of X(S2) and much higher than that of X(S1) across the entire spectrum. This is consistent with transport results, where the ionic conductivity of X(S1+S2) matches X(S2) and is double that of X(S1).[9,10] These findings indicate that PEO chain vibrations are closely linked to ionic transport, and the addition of salts can modify the vibrational properties of PEO chains. In summary, choosing the appropriate salt proportion can notably alter the crystallinity of SPEs, thereby affecting their vibrational and transport properties. THz-TDS is, thus, an indispensable tool for investigating the vibrational properties of polymer chains and establishing a connection to transport data.

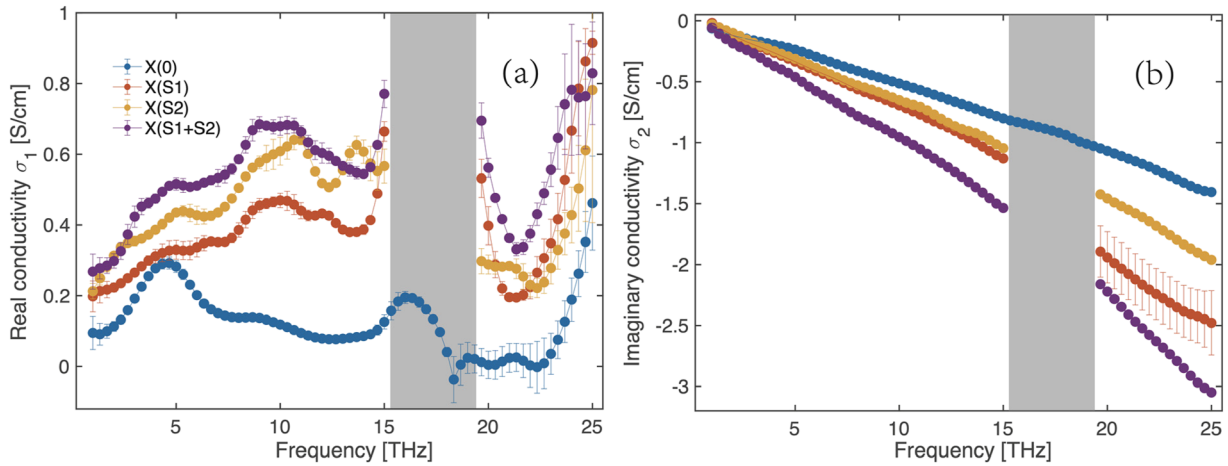

FIG. 2. (a) The real part and (b) the imaginary part of frequency-dependent conductivity spectra of pure cross-linked polymer X(0), single-salt-doped electrolytes X(S1) [LiTFSI] and X(S2) [LiDFOB], and dual-salt-doped electrolytes X(S1+S2) [LiTFSI+LiDFOB] samples. The spectra of X(S1), X(S2), and X(S1+S2) in the range marked with gray are affected by the phonon absorption in the silicon wafer filter, and their high absorption exceeds the reliable measurement limit.

B. Infrared spectra

Figure 3(a) shows the transmission spectra of the samples, with the fundamental vibrational modes of PEO and the lithium salts indicated by solid lines. Most of these modes are too intense to allow direct observation of their central frequencies, as their strong absorption prevents radiation from transmitting through the samples and thereby hinders accurate assessment. To address this limitation, we employed Attenuated Total Reflectance (ATR)-FTIR measurements to examine the fundamental vibrational modes (see Note 4 and Fig. S3 in the supplementary material). By using ATR-FTIR spectroscopy and building on previous research,[22,23,28–43] we were able to determine the central frequencies of these modes.

The obtained results align well with previous studies,[22,23,28–43] and the detailed information is available in Table I. In the range of 730–790 cm^{-1}, three stretching vibration modes of LiTFSI salts are observable only in the LiTFSI-doped samples, X(S1) and X(S1+S2) [Fig. 3(b)]. The strong, broad absorption band from 840 to 1500 cm^{-1} primarily arises from the vibrational modes of PEO.[30,31] The strongest vibrational band is the C–O–C stretching mode at 1097 cm^{-1} (supplementary material, Note 4), which can be used to assess PEO crystallinity and to understand the coordination of ions with PEO chains, in agreement with earlier reports.[38–40] The CH_2 twisting modes are observed at 1240 and 1278 cm^{-1}, while the bending modes of CH_2 are observed at 1342, 1359, and 1466 cm^{-1}, also in agreement with the literature.[41–43] These fundamental modes are exceptionally strong, exceeding the detection limit of our spectrometer, resulting in minimal observable feature variation among the samples in this range. The vibrational band at 1720 cm^{-1} is related to the C=O stretching mode, which may arise from the initiator decomposition or side reaction during the crosslinking process.[37] Another

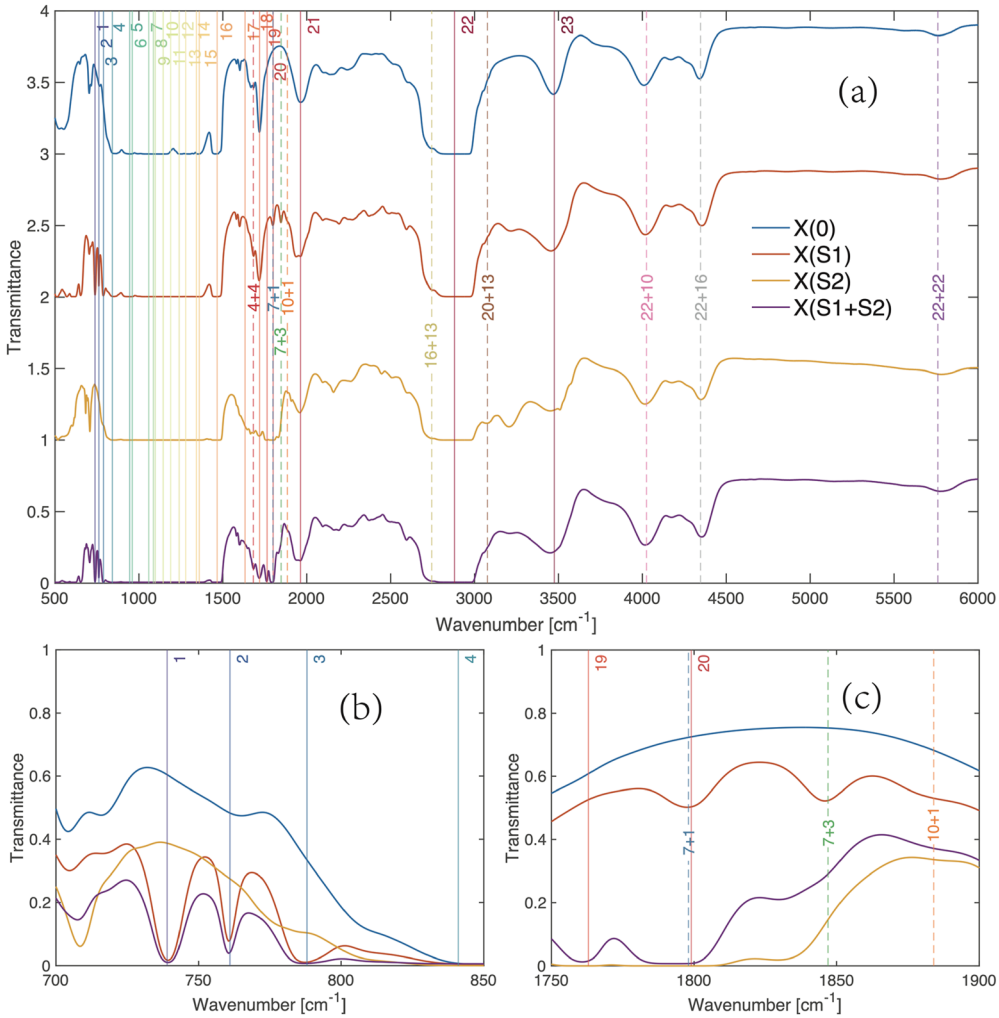

FIG. 3. FTIR transmission spectra of SPEs. The vertical lines, ranging from small to large and shifting from blue to red, indicate the positions of the fundamental vibrations. Detailed information is available in Table I. The vertical dashed lines denote the positions of overtones or combination modes, labeled with "x+y," indicating their origin from the superposition of the "x" and "y" vibrations. In (a), the vertical axes of different samples have been vertically translated by 1 to aid in distinction. [(b) and (c)] are partial enlargements of (a), with no vertical translation applied to the transmission (the y-axis).

TABLE I. Vibrational modes of SPEs observed in FTIR experiments. The numbered entries correspond to those depicted in Fig. 3. Wavenumber values indicate FTIR transmission bands for various vibrational modes of groups present in PEO, LiTFSI, and LiDFOB, classified as stretching ν, bending δ, rocking ρ, and twisting τ, while assignment of mode 21 remains debated.[22,23,28–43]

Mode order	Wavenumber (cm^{-1})	Vibrational mode	Origin
1	739	ν S–N	LiTFSI
2	761	ν C–S, ν C–F	LiTFSI
3	788	ν C–S, ν C–F	LiTFSI
4	841	ρ CH_2	PEO
5	945	ν C–O	PEO
6	960	ν C–O	PEO
7	1059	ν C–O–C	PEO
8	1086	ν F–B–F	LiDFOB
9	1097	ν C–O–C	PEO
10	1145	ν C–O–C	PEO
11	1190	ν CF_3	LiTFSI
12	1240	τ CH_2	PEO
13	1278	τ CH_2	PEO
14	1342	δ CH_2	PEO
15	1359	δ CH_2	PEO
16	1466	δ CH_2	PEO
17	1633	ν B–F	LiDFOB
18	1720	ν C=O	Crosslinking process
19	1763	ν C=O	LiDFOB
20	1799	ν C=O	LiDFOB
21	1963	tentative/ debated[28,35,36]	PEO
22	2880	ν C–H	PEO
23	3475	ν O–H	Water

strong absorption band, found between 2700 and 2950 cm^{-1}, corresponds to the symmetric and asymmetric C–H stretching modes of the CH_2 group in PEO.[31] In addition, a prominent vibration mode at 3475 cm^{-1} is attributed to the O–H stretching mode, likely due to H_2O molecules introduced during production or storage. Similar vibrational bands have been noted in previous studies of PEO and PEO-based SPEs.[22,23,28–43]

Beyond these well-assigned fundamental modes, there are three clear vibrational bands above 4000 cm^{-1} in Fig. 3(a), which cannot be captured from the fundamental vibrations of any components inside SPEs. In fact, 4000 cm^{-1} is the conventional borderline between the mid-IR and near-IR. The fundamental vibrational frequency higher than 4000 cm^{-1} can only be attributed to H_2 (4160 cm^{-1}); however, this mode is only Raman active and not IR active; hence, it cannot be observed in an IR spectrum.[44] In the near-IR region, the overtones and combination modes are the main contributors. Because they originate from the anharmonic effect, they are much weaker than the fundamental vibrational modes [Fig. 3]. Anharmonicity of the molecular vibration is a result of asymmetric non-parabolic intermolecular potential, which is distinguished from the quadratic (or parabolic) potential characteristic of a harmonic oscillator with its equally spaced energy levels and perfectly symmetric or antisymmetric wavefunctions[44,45] (see also the schematic illustration in Note 6 of the supplementary material). By carefully comparing the vibrational frequencies, we find that the three vibrational modes above 4000 cm^{-1} originate from the coupling of the fundamental vibrational modes in PEO. Specifically, the mode at 4022 cm^{-1} (labeled as "22 + 10") is the combination mode of the stretching mode of C–H (2880 cm^{-1} labeled as "22") and C–O–C (1059 cm^{-1} labeled as "10") of PEO, the mode at 4346 cm^{-1} (labeled as "22 + 16") is the combination mode of the stretching mode of C–H (2880 cm^{-1} labeled as "22") and the bending mode of CH_2 (1466 cm^{-1} labeled as "16") of PEO, and the mode at 5760 cm^{-1} (labeled as "22 + 22") is the first overtone of the stretching mode of C–H (2880 cm^{-1} labeled as "22"). All modes exhibit a slight blue shift in the SPE spectra compared to the pure PEO spectrum. This shift may result from the hardening of the vibrational potential due to the incorporation of lithium salts.[23]

By considering overtones and combination modes, we can interpret the IR transmission spectra more comprehensively and gain a better understanding of the interactions within SPEs. Previous studies have demonstrated and analyzed the interaction between lithium salts and PEO by observing shifts in fundamental vibration frequency and changes in intensity.[23,30,34] However, these shifts are often small, and when fundamental vibrations are too strong, it becomes challenging to observe such frequency shifts.[23,30] In this context, the combination modes from PEO and lithium salts directly indicate their interactions. In addition, they help identify the specific functional groups involved in these interactions. For example, in X(S2), a combination mode labeled as "20 + 13" arises from the stretching vibration of C=O in LiDFOB (1799 cm^{-1} labeled as "20") and the twisting vibration of CH_2 in PEO (1278 cm^{-1} labeled as "13"). This plausibly indicates the formation of hydrogen bonds (C–H···O=C) between PEO and $DFOB^-$ anions. The frequency shift of the C–H fundamental vibration mode was also observed in previous studies, suggesting the formation of hydrogen bonds between PEO and lithium salts.[34,46,47]

Similar effects are observed with LiTFSI-doped PEO, as shown in Figs. 3(b) and 3(c). In X(S1), the combination modes involving the stretching modes of S–N and C–S from LiTFSI and C–O–C from PEO are evident. As expected, the higher frequency modes exhibit greater transparency compared to lower frequency modes, due to the weaker intensity of combination modes originating from anharmonicity, as compared to the fundamental vibration modes [Figs. 3(b) and 3(c)]. Interestingly, the frequency of the combination mode "7 + 1" is close to the fundamental vibration of the C=O stretching mode (labeled as "20") in LiDFOB. Even a small addition of 3 wt. % LiDFOB in the dual-salt-doped sample X(S1+S2) notably alters the spectrum in this range compared to X(S1) and is comparable to the spectrum of the 14 wt. % LiDFOB-doped sample X(S2). This demonstrates that introducing a new type of salt can alter the properties of SPEs, consistent with findings from transport and THz spectroscopy measurements mentioned earlier.

We acknowledge that similar bands have been noted in previous studies but were often overlooked due to their weak intensity.[30,32] Our ability to observe these stronger overtones and combination modes is likely due to our sample being ~300 μm thick, which is 2–6 times thicker than those used in earlier research (50–150 μm).[30,32] Overtones and combination modes provide additional insights into the interactions between PEO and lithium salts that cannot be directly obtained from analyzing fundamental

vibrational modes alone. We also investigate the temperature-dependent behavior of the anharmonic vibrational modes from X(0) and X(S1). It shows that within the temperature range of our FTIR measurements, the absorption spectrum of our PEO-based SPEs only changed slightly with a change of temperature between 20 and 50 °C (supplementary material, Note 5), which reflects the excellent thermal stability of PEO as an electrolyte for lithium-ion batteries.[5] To further substantiate that these vibrational modes originate from the anharmonicity effects, we carried out the DFT calculations, as discussed in Sec. III C.

C. Density functional theory (DFT) calculation

Quantum mechanical DFT calculations of vibrational transitions are highly effective in elucidating the results of infrared spectroscopy.[44,48] These calculations allow for the determination of spectral positions and absorption intensities of vibrational modes. Our DFT calculations were performed using the Gaussian16 package.[49] The molecular structures were optimized with the B3LYP DFT functional and the 6–311++G(d, p) basis set. To simulate the effect of a surrounding electrolyte, a solvation model using parameters for diethyl ether was employed, as it has a dielectric constant (ε = 4.24) similar to that of PEO.[50,51] The xQC SCF convergence criterion and an ultrafine integration grid were utilized for the calculations. Both harmonic and anharmonic DFT calculations are applied to the PEO molecule, as depicted in Fig. 4. In the calculations with harmonic potentials, only fundamental vibrational modes are considered, while overtones and combination modes are excluded under the harmonic-oscillator approximation. Consequently, as shown in Fig. 4, the calculated vibrational intensity is zero above 4000 cm^{-1} in the harmonic calculation. In addition, there is a noticeable blue shift between the calculated and experimental data around 2800 cm^{-1}, corresponding to the C–H stretching mode. This discrepancy may arise from intra- and inter-molecular interactions, which are not captured by harmonic calculations. In addition, the polymer chain used in the DFT calculations is shorter than that of the actual samples used in the experiment due to limitations in software calculation capacity and speed.

By considering anharmonicity in the calculations, incorporating contributions from overtones and combination modes, we achieve a closer match with the experimental data. Furthermore, the calculations reveal non-zero vibrational intensities above 4000 cm^{-1}. The DFT calculations thus support our experimental findings, supporting the assignment of signals to overtones and combination modes within SPEs.

D. IR–UV spectra

The photometric IR–UV transmission data are shown in Fig. 5(a). The vibration modes in the IR region reproduced the experimental results of the FTIR spectra. In addition, we observe a sharp transition in the UV region, which is referred to as the optical transition from bonding to an anti-bonding state.[23,52–54] The power absorption coefficient $\alpha(\omega)$ can be extracted from the absorbance $A(\omega)$,

$$\alpha(\omega) = \frac{2.303}{x} \log\left(\frac{I_0}{I}\right) = \frac{2.303}{x} A(\omega) \ , \tag{1}$$

where x is the sample thickness, and I_0 and I are the incident and transmitted intensities, respectively.[55] The absorption coefficient $\alpha(\omega)$ for noncrystalline materials can be related to the energy of the incident photon ($h\nu$) according to the formula

$$(\alpha h\nu)^m = B(h\nu - E_g) \ , \tag{2}$$

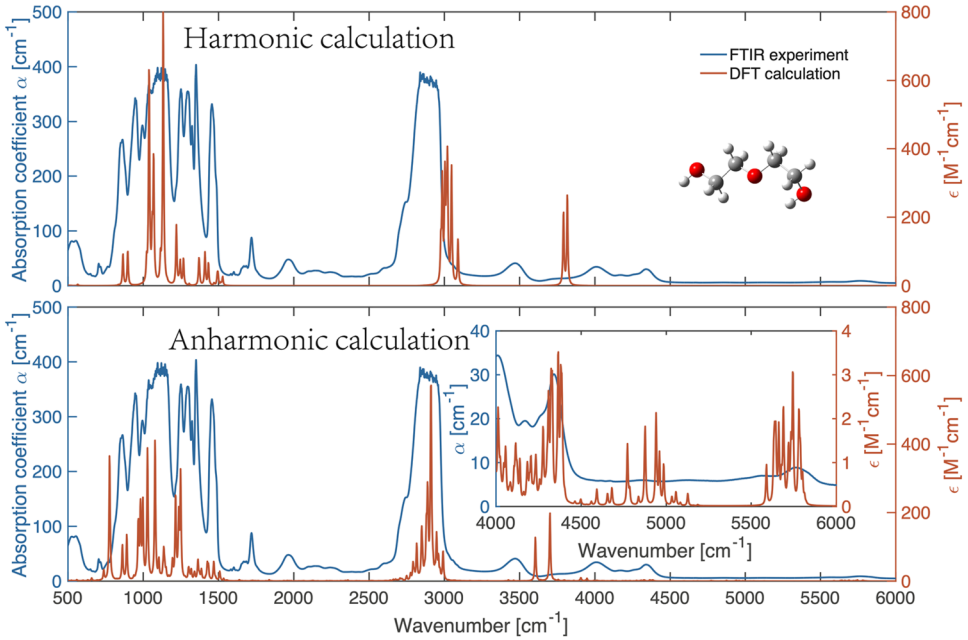

FIG. 4. Comparison of DFT calculations with the experimentally determined absorption coefficient of the sample X(0). Upper panel: The harmonic DFT calculation vs experimental data. The inset is the molecule cluster used in the calculation. Lower panel: The anharmonic DFT calculation vs experimental data. The inset is the zoomed-in image of the anharmonic calculation in the spectral range 4000–6000 cm^{-1}.

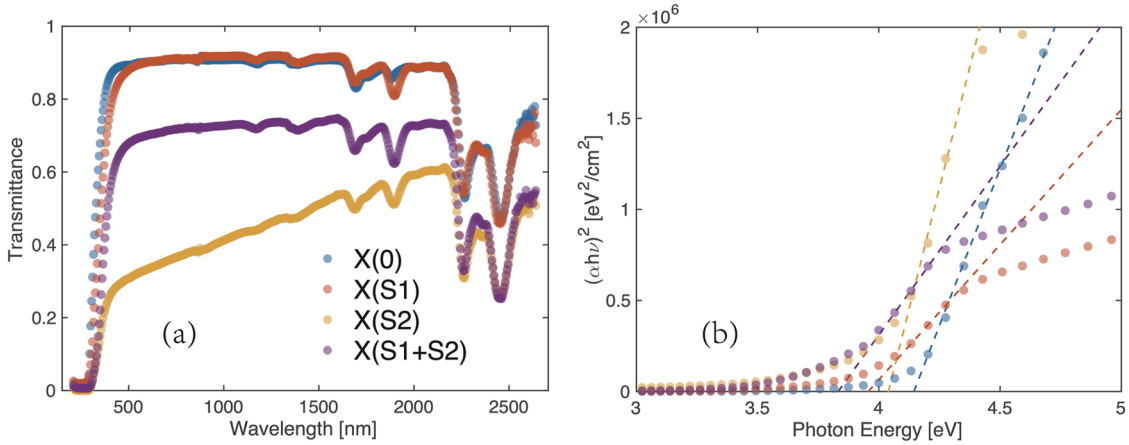

FIG. 5. Photometric IR–UV spectra of SPE samples. (a) The IR–UV transmission spectrum of SPE samples from 2640 nm (0.470 eV) to 210 nm (5.904 eV). (b) $(\alpha h\nu)^2$ vs photon energy for SPE samples. The solid–dashed lines are the linear fits of the data with the same color.

where h is the Planck constant, ν is the photon wave frequency, B is a material constant independent of the energy gap, E_g is the optical bandgap energy, and m is the power factor of $m = 2$ for the direct gap transitions and $m = 1/2$ for the indirect gap transitions.[23,55–57]

The momentum of a photon is negligible compared to that of an electron in a solid. In direct-gap transitions, an electron absorbs a photon and transitions to a higher energy level without a change in momentum. However, in indirect gap transitions, a change in momentum is required, typically involving the assistance of a phonon. As a result, indirect gap transitions are considered second-order processes and, for this reason, are much weaker than direct gap transitions. In spectroscopy, direct gap transitions are characterized by sharp change features, while indirect-gap transitions exhibit more gradual changes.

To determine the gap energy for the electronic transition in each sample, we follow a common protocol based on the Tauc plot.[23,53,58] Hence, we draw the function $(\alpha h\nu)^2$, corresponding to direct gap transition vs photon energy $(h\nu)$, and fit the data with a linear function, as shown in Fig. 5(b). The intersection of the fitted line with the horizontal axis provides the direct gap energy of the sample as referred to in Eq. (2). The results are summarized in Table II. The addition of lithium salts results in a smaller direct energy gap, as compared to that of the bare PEO, with the dual-salt-doped sample exhibiting the smallest direct energy gap. This reduction in the energy gap can plausibly be attributed to additional electronic transition channels arising from unsaturated bonds or unoccupied states introduced into the PEO bandgap, induced by the molecular anion of the added salt, LiTFSI in X(S1) and LiDFOB in X(S2). It is also realized that the induced reduction of the optical energy gap is the strongest in the case of the LiTFSI-doped system, consistent with earlier studies.[23,53,59] In addition, the change in the optical energy gap indicates interactions between the lithium salts and PEO chains. This interaction leads to the formation of localized states within the forbidden energy bandgap of the polymer matrix, resulting from ion–dipole interactions.[23] This reduction of the bandgap induced by the added salt is expected to have a significant negative impact on the electrolyte performance in batteries, as it leads to a reduction of the electronic resistivity of the electrolyte, which in turn increases the leakage current in a battery cell.[8,9,59] We further observe that in the range of 500–2640 nm, the transmission of X(S2) and X(S1+S2) is lower compared to X(0) and X(S1). Upon examining the electron microscope images of these samples (supplementary material, Note 7), we found that X(S2) and X(S1+S2) contain more scattering centers, with X(S2) being the most pronounced. This suggests that the reduced optical transmission in this range is primarily due to optical scattering within the samples.

TABLE II. Direct gap energy of SPE samples.

	X(0)	X(S1)	X(S2)	X(S1+S2)
Direct gap energy (eV)	4.14	3.92	4.04	3.83

IV. CONCLUSIONS

Optical spectroscopy plays a crucial role in studying the properties of SPEs. Using ultrabroadband THz pulses, we can characterize the vibrations of PEO chains. In the THz spectrum, the broadening of vibrational modes with the addition of lithium salts corresponds to the increased amorphous phases introduced by the salts. The THz conductivity of the dual-salt-doped sample X(S1+S2), containing only 3 wt. % LiDFOB, is notably higher than that of the single-salt-doped sample X(S1) with the same EO: Li^+ ratio, aligning well with the transport measurements that show twice the ionic conductivity for X(S1+S2) as compared to X(S1). This highlights the role of the polymer chain dynamics in facilitating the lithium-ion transport and hence the DC ionic conductivity. In the IR range, vibrations of chemical bonds within polymer chains and lithium salts are predominant. By analyzing overtones and combination modes, we gain deeper insights into the IR spectrum. Anharmonic vibration modes reveal interactions between lithium salts and PEO chains,

identifying specific functional groups involved. By taking anharmonic effects into account, DFT calculations yielded results that are more consistent with experimental results, helping to assign the overtones and combination modes. Further analysis of these anharmonic vibrations in SPEs, which have been overlooked in previous studies, is warranted. In the UV/Vis range, we characterize the optical gap energy. The addition of lithium salts decreases the optical gap energy, with the dual-salt-doped sample X(S1+S2) having the smallest gap, suggesting the formation of additional electronic conduction channels. Our optical studies enhance the understanding of SPEs and can plausibly contribute to advancements in solid-state lithium-ion battery applications and ongoing efforts to improve the properties of SPEs.

SUPPLEMENTARY MATERIAL

The supplementary material includes Note 1: Air-photonics THz spectrometer; Note 2: Data analysis for the ultrabroadband THz spectroscopy; Note 3: Transport parameters of PEO-based SPEs; Note 4: Attenuated Total Reflectance (ATR)-FTIR spectroscopy; Note 5: Temperature-dependent FTIR spectroscopy; Note 6: Schematic illustration of anharmonic and harmonic potentials; Note 7: Microscopic image of samples.

ACKNOWLEDGMENTS

The authors acknowledge fruitful discussions with Tomoki Hiraoka and the financial support from the European Union's Horizon 2020 research and innovation program (Grant Agreement No. 964735 EXTREME-IR), Deutsche Forschungsgemeinschaft (DFG) within Project No. 468501411-SPP2314 INTEGRATECH under the framework of the priority program SPP2314-INTEREST, and within Project No. 518575758 HIGHSPINTERA, Bundesministerium für Bildung und Forschung (BMBF) within Project No. 05K2022 PBA Tera-EXPOSE and Project No. 13XP5129 EFoBatt.

AUTHOR DECLARATIONS

Conflict of Interest

The authors have no conflicts to disclose.

Author Contributions

H. Hafez, M. Baghernejad, and D. Turchinovich conceived the idea and supervised the project. J. Wang and F. Pfeiffer prepared the samples. Y. Meng, H. Hafez, and W. Zhang constructed the in-house THz spectrometer and performed the THz-TDS measurements. Y. Meng and L. Goett-Zink performed the room temperature FTIR measurements under the supervision of T. Kottke. J. Wang performed temperature-dependent FTIR and ATR-FTIR measurements. Y. Meng performed the photometric IR–UV spectroscopy and performed the data analysis for the whole study. M. Weiling performed the DFT calculations. Y. Meng and H. Hafez wrote the paper with contributions from M. Baghernejad and D. Turchinovich. All co-authors discussed the results and commented on the paper.

Yuhao Meng: Data curation (equal); Formal analysis (equal); Investigation (equal); Methodology (equal); Software (equal); Validation (equal); Writing – original draft (equal); Writing – review & editing (equal). **Jian-Fen Wang**: Data curation (equal); Formal analysis (equal); Investigation (equal); Methodology (equal); Writing – review & editing (equal). **Matthias Weiling**: Data curation (equal); Formal analysis (equal); Investigation (equal); Methodology (equal); Software (equal); Writing – review & editing (equal). **Wentao Zhang**: Investigation (equal); Methodology (equal). **Felix Pfeiffer**: Data curation (equal); Investigation (equal); Methodology (equal); Writing – review & editing (equal). **Lukas Goett-Zink**: Data curation (equal); Investigation (equal); Writing – review & editing (equal). **Tilman Kottke**: Investigation (equal); Resources (equal); Supervision (equal); Writing – review & editing (equal). **Jijeesh Ravi Nair**: Investigation (equal); Writing – review & editing (equal). **Masoud Baghernejad**: Conceptualization (equal); Data curation (equal); Funding acquisition (equal); Investigation (equal); Methodology (equal); Resources (equal); Supervision (equal); Writing – review & editing (equal). **Dmitry Turchinovich**: Conceptualization (equal); Data curation (equal); Funding acquisition (equal); Investigation (equal); Methodology (equal); Resources (equal); Supervision (equal); Validation (equal); Writing – review & editing (equal). **Hassan A. Hafez**: Conceptualization (equal); Data curation (equal); Formal analysis (equal); Investigation (equal); Methodology (equal); Supervision (equal); Validation (equal); Writing – original draft (equal); Writing – review & editing (equal).

DATA AVAILABILITY

The data that support the findings of this study are available within the article and its supplementary material.

REFERENCES

[1] D. Deng, "Li-ion batteries: Basics, progress, and challenges," Energy Sci. Eng. **3**, 385 (2015).
[2] M.-H. Chiou, E. Verweyen, D. Diddens, L. Wichmann, C. Schmidt, K. Neuhaus, A. Choudhary, D. Bedrov, M. Winter, and G. Brunklaus, "Selection of polymer segment species matters for electrolyte properties and performance in lithium metal batteries," ACS Appl. Energy Mater. **6**, 4422 (2023).
[3] Z. Xue, D. He, and X. Xie, "Poly(ethylene oxide)-based electrolytes for lithium-ion batteries," J. Mater. Chem. A **3**, 19218 (2015).
[4] H. Yang and N. Wu, "Ionic conductivity and ion transport mechanisms of solid-state lithium-ion battery electrolytes: A review," Energy Sci. Eng. **10**, 1643 (2022).
[5] D. Brandell, J. Mindemark, and G. Hernández, *Polymer-based Solid State Batteries* (Walter de Gruyter GmbH & Co KG, 2021).
[6] K. E. Aifantis, S. A. Hackney, and R. V. Kumar, *High Energy Density Lithium Batteries* (Wiley Online Library, 2010).
[7] F. Croce, G. B. Appetecchi, L. Persi, and B. Scrosati, "Nanocomposite polymer electrolytes for lithium batteries," Nature **394**, 456 (1998).
[8] Z. Gadjourova, Y. G. Andreev, D. P. Tunstall, and P. G. Bruce, "Ionic conductivity in crystalline polymer electrolytes," Nature **412**, 520 (2001).
[9] I. Shaji, D. Diddens, N. Ehteshami, M. Winter, and J. R. Nair, "Multisalt chemistry in ion transport and interface of lithium metal polymer batteries," Energy Storage Mater. **44**, 263 (2022).
[10] J. Weidelt, J. R. Nair, D. Diddens, W. Zhang, F. Pfeiffer, T. de Oliveira Schneider, M. Meinert, T. Hiraoka, L. Nesterov, M. Baghernejad *et al.*, "Fundamental picture of the conduction mechanism in solid-state polymer electrolytes revealed by terahertz spectroscopy," J. Phys. Chem. C **128**, 6868 (2024).
[11] A. Maitra and A. Heuer, "Cation transport in polymer electrolytes: A microscopic approach," Phys. Rev. Lett. **98**, 227802 (2007).
[12] K.-J. Lin and J. K. Maranas, "Cation coordination and motion in a poly(ethylene oxide)-based single ion conductor," Macromolecules **45**, 6230 (2012).
[13] D. J. Brooks, B. V. Merinov, W. A. Goddard III, B. Kozinsky, and J. Mailoa, "Atomistic description of ionic diffusion in PEO–LiTFSI: Effect of temperature, molecular weight, and ionic concentration," Macromolecules **51**, 8987 (2018).

[14]S. Li, Y.-M. Chen, W. Liang, Y. Shao, K. Liu, Z. Nikolov, and Y. Zhu, "A superionic conductive, electrochemically stable dual-salt polymer electrolyte," Joule **2**, 1838 (2018).
[15]L. Long, S. Wang, M. Xiao, and Y. Meng, "Polymer electrolytes for lithium polymer batteries," J. Mater. Chem. A **4**, 10038 (2016).
[16]C. F. Klingshirn, *Semiconductor Optics* (Springer Science & Business Media, 2012).
[17]M. Dressel and G. Grüner, *Electrodynamics of Solids: Optical Properties of Electrons in Matter* (Cambridge University Press, 2002).
[18]V. Vijayakumar, D. Diddens, A. Heuer, S. Kurungot, M. Winter, and J. R. Nair, "Dioxolanone-anchored poly(allyl ether)-based cross-linked dual-salt polymer electrolytes for high-voltage lithium metal batteries," ACS Appl. Mater. Interfaces **12**, 567 (2019).
[19]X. Xie, J. Dai, and X.-C. Zhang, "Coherent control of THz wave generation in ambient air," Phys. Rev. Lett. **96**, 075005 (2006).
[20]N. Karpowicz, J. Dai, X. Lu, Y. Chen, M. Yamaguchi, H. Zhao, X.-C. Zhang, L. Zhang, C. Zhang, M. Price-Gallagher, C. Fletcher, O. Mamer, A. Lesimple, and K. Johnson, "Coherent heterodyne time-domain spectrometry covering the entire "terahertz gap," Appl. Phys. Lett. **92**, 011131 (2008).
[21]F. D'Angelo, Z. Mics, M. Bonn, and D. Turchinovich, "Ultra-broadband THz time-domain spectroscopy of common polymers using THz air photonics," Opt. Express **22**, 12475 (2014).
[22]U. Sasikala, P. N. Kumar, V. Rao, and A. Sharma, "Structural, electrical and parametric studies of a PEO based polymer electrolyte for battery applications," Int. J. Eng. Sci. Adv. Technol. **2**, 722 (2012).
[23]R. J. Sengwa, V. K. Patel, and M. Saraswat, "Investigation on promising properties of PEO/PVP/LiTFSI solid polymer electrolytes for high-performance energy storage and next-generation flexible optoelectronic and iontronic devices," J. Polym. Res. **29**, 480 (2022).
[24]A. R. Polu, S. Song, A. A. Kareem, S. V. Savilov, P. K. Singh, M. Venkanna, and C. S. Kumar, "Performance enhancement of PEO: LiDFOB based nanocomposite solid polymer electrolytes via incorporation of POSS-$PEG_{13.3}$ hybrid nanoparticles for solid-state Li-ion batteries," J. Phys. Chem. Solids **196**, 112319 (2025).
[25]A. R. Polu, D. K. Kim, and H.-W. Rhee, "Poly(ethylene oxide)-lithium difluoro(oxalato)borate new solid polymer electrolytes: Ion–polymer interaction, structural, thermal, and ionic conductivity studies," Ionics **21**, 2771 (2015).
[26]E. K. W. Andersson, L.-T. Wu, L. Bertoli, Y.-C. Weng, D. Friesen, K. Elbouazzaoui, S. Bloch, R. Ovsyannikov, E. Giangrisostomi, D. Brandell *et al.*, "Initial SEI formation in LiBOB-LiDFOB- and $LiBF_4$-containing PEO electrolytes," J. Mater. Chem. A **12**, 9184 (2024).
[27]M. Ghelichi, N. T. Qazvini, S. H. Jafari, H. A. Khonakdar, Y. Farajollahi, and C. Scheffler, "Conformational, thermal, and ionic conductivity behavior of PEO in PEO/PMMA miscible blend: Investigating the effect of lithium salt," J. Appl. Polym. Sci. **129**, 1868 (2013).
[28]B. L. Papke, M. A. Ratner, and D. F. Shriver, "Vibrational spectroscopic determination of structure and ion pairing in complexes of poly(ethylene oxide) with lithium salts," J. Electrochem. Soc. **129**, 1434 (1982).
[29]S. J. Wen, T. J. Richardson, D. I. Ghantous, K. A. Striebel, P. N. Ross, and E. J. Cairns, "FTIR characterization of PEO + $LiN(CF_3SO_2)_2$ electrolytes," J. Electroanal. Chem. **408**, 113 (1996).
[30]V. M. Mohan, P. B. Bhargav, V. Raja, A. K. Sharma, and V. V. R. Narasimha Rao, "Optical and electrical properties of pure and doped PEO polymer electrolyte films," Soft Mater. **5**, 33 (2007).
[31]V. M. Mohan, V. Raja, P. B. Bhargav, A. K. Sharma, and V. V. R. N. Rao, "Structural, electrical and optical properties of pure and $NaLaF_4$ doped PEO polymer electrolyte films," J. Polym. Res. **14**, 283 (2007).
[32]X. Li, Z. Wang, H. Lin, Y. Liu, Y. Min, and F. Pan, "Composite electrolytes of pyrrolidone-derivatives-PEO enable to enhance performance of all solid state lithium-ion batteries," Electrochim. Acta **293**, 25 (2019).
[33]K. Kim, L. Kuhn, I. V. Alabugin, and D. T. Hallinan, Jr., "Lithium salt dissociation in diblock copolymer electrolyte using Fourier transform infrared spectroscopy," Front. Energy Res. **8**, 569442 (2020).
[34]S. Wang, Q. Sun, Q. Zhang, C. Li, C. Xu, Y. Ma, X. Shi, H. Zhang, D. Song, and L. Zhang, "Li-ion transfer mechanism of ambient-temperature solid polymer electrolyte toward lithium metal battery," Adv. Energy Mater. **13**, 2204036 (2023).
[35]A. M. Stephan, T. P. Kumar, M. A. Kulandainathan, and N. A. Lakshmi, "Chitin-Incorporated poly(ethylene oxide)-based nanocomposite electrolytes for lithium batteries," J. Phys. Chem. B **113**, 1963 (2009).
[36]S. Rajendran, R. Kannan, and O. Mahendran, "Ionic conductivity studies in poly(methylmethacrylate)–polyethlene oxide hybrid polymer electrolytes with lithium salts," J. Power Sources **96**, 406 (2001).
[37]A. Papagiannopoulos, E. Vlassi, S. Pispas, C. Tsitsilianis, and A. Radulescu, "Polyethylene oxide hydrogels crosslinked by peroxide for the controlled release of proteins," Macromol **1**, 37 (2020).
[38]O. Guchok, G. Ardel, T. D. Keidar, H. Nakar, H. Ragones, D. Kaplan, A. Zheng, S. Greenbaum, I. Lounev, A. Greenbaum *et al.*, "Understanding of the ion transport in blended TPU-PEO polymer electrolytes," J. Solid State Electrochem. (published online 2025).
[39]S. Ibrahim, M. M. Yassin, R. Ahmad, and M. R. Johan, "Effects of various $LiPF_6$ salt concentrations on PEO-based solid polymer electrolytes," Ionics **17**, 399 (2011).
[40]D. Saikia, C.-G. Wu, J. Fang, L.-D. Tsai, and H.-M. Kao, "Organic–inorganic hybrid polymer electrolytes based on polyether diamine, alkoxysilane, and trichlorotriazine: Synthesis, characterization, and electrochemical applications," J. Power Sources **269**, 651 (2014).
[41]P. Dhatarwal and R. J. Sengwa, "Influence of solid polymer electrolyte preparation methods on the performance of (PEO–PMMA)–$LiBF_4$ films for lithium-ion battery applications," Polym. Bull. **75**, 5645 (2018).
[42]S. Yang, Z. Liu, Y. Liu, and Y. Jiao, "Effect of molecular weight on conformational changes of PEO: An infrared spectroscopic analysis," J. Mater. Sci. **50**, 1544 (2015).
[43]D. E. Hegazy and G. A. Mahmoud, "Radiation synthesis and characterization of polyethylene oxide/chitosan-silver nanocomposite for biomedical applications," Arab J. Nucl. Sci. Appl. **47**, 1 (2014).
[44]Y. Ozaki, C. Huck, S. Tsuchikawa, and S. B. Engelsen, *Near-infrared Spectroscopy: Theory, Spectral Analysis, Instrumentation, and Applications* (Springer Nature, 2020).
[45]M. Fox, *Optical Properties of Solids* (Oxford University Press, 2010).
[46]K. Müller-Dethlefs and P. Hobza, "Noncovalent interactions: A challenge for experiment and theory," Chem. Rev. **100**, 143 (2000).
[47]Z. Hu, F. Xian, Z. Guo, C. Lu, X. Du, X. Cheng, S. Zhang, S. Dong, G. Cui, and L. Chen, "Nonflammable nitrile deep eutectic electrolyte enables high-voltage lithium metal batteries," Chem. Mater. **32**, 3405 (2020).
[48]M. A. Czarnecki, Y. Morisawa, Y. Futami, and Y. Ozaki, "Advances in molecular structure and interaction studies using near-infrared spectroscopy," Chem. Rev. **115**, 9707 (2015).
[49]M. E. Frisch, G. Trucks, H. B. Schlegel, G. Scuseria, M. Robb, J. Cheeseman, G. Scalmani, V. Barone, G. Petersson, and H. Nakatsuji, *Gaussian 16, Revision C.01*, Gaussian, Inc., Wallingford, CT, 2016.
[50]A. V. Marenich, C. J. Cramer, and D. G. Truhlar, "Universal solvation model based on solute electron density and on a continuum model of the solvent defined by the bulk dielectric constant and atomic surface tensions," J. Phys. Chem. B **113**, 6378 (2009).
[51]F. Faglioni, B. V. Merinov, W. A. Goddard, and B. Kozinsky, "Factors affecting cyclic durability of all-solid-state lithium batteries using poly(ethylene oxide)-based polymer electrolytes and recommendations to achieve improved performance," Phys. Chem. Chem. Phys. **20**, 26098 (2018).
[52]M. Basappa, L. Yesappa, M. Niranjana, S. P. Ashokkumar, M. Vandana, H. Vijeth, and H. Devendrappa, AIP Conf. Proc. **1953**, 030095 (2018).
[53]R. S. Al-Faleh and A. M. Zihlif, "A study on optical absorption and constants of doped poly(ethylene oxide)," Physica B **406**, 1919 (2011).
[54]M. A. Al-Akhras, M. Telfah, M. N. Shakhatreh, A. Telfah, M. S. Mousa, V. Narayanaswamy, and I. M. Obaidat, "Optical and chemical investigations of PEO thin films incorporated with curcumin nanoparticle: Effect of film thickness," Biointerface Res. Appl. Chem. **13**, 143 (2023).
[55]R. J. Borg and G. J. Dienes, *The Physical Chemistry of Solids* (Academic Press, 1992).

[56]E. A. Davis and N. F. Mott, "Conduction in non-crystalline systems V. Conductivity, optical absorption and photoconductivity in amorphous semiconductors," Philos. Mag. **22**, 0903 (1970).
[57]J. Tauc, *Amorphous and Liquid Semiconductors* (Springer Science & Business Media, 2012).
[58]J. Tauc, "Optical properties and electronic structure of amorphous Ge and Si," Mater. Res. Bull. **3**, 37 (1968).
[59]M. Unge, H. Gudla, C. Zhang, and D. Brandell, "Electronic conductivity of polymer electrolytes: Electronic charge transport properties of LiTFSI-doped PEO," Phys. Chem. Chem. Phys. **22**, 7680 (2020).